

# Wrinkling of Random and Regular Semiflexible Polymer Networks

Pascal Müller and Jan Kierfeld

*Physics Department, TU Dortmund University, 44221 Dortmund, Germany*

(Dated: September 20, 2018)

We investigate wrinkling of two-dimensional random and triangular semiflexible polymer networks under shear. Both types of semiflexible networks exhibit wrinkling above a small critical shear angle, which scales with an exponent of the bending modulus between 1.9 and 2.0. Random networks exhibit hysteresis at the wrinkling threshold. Wrinkling lowers the total elastic energy by up to 20% and strongly affects the elastic properties of all semiflexible networks such as the crossover between bending and stretching dominated behavior. In random networks, we also find evidence for metastable wrinkled configurations. While the disordered microstructure of random networks affects the scaling behavior of wrinkle amplitudes, it has little effect on wrinkle wavelength. Therefore, wrinkles represent a robust, microstructure-independent assay of shear strain or elastic properties.

PACS numbers: 46.32.+x, 87.16.Ka, 87.16.dm, 46.70.De

Random networks of stiff fibers or polymers are important model systems for biopolymer meshworks in the cell cortex or the cytoplasm [1] or synthetic nanofibrous materials [2]. In such a network structure, a random array of fibers or semiflexible polymers with an intrinsic bending rigidity is cross-linked. We will focus on the situation where cross-linking is permanent on the time scale of network deformation. Quasi-two-dimensional (2D) geometries are used to model sheetlike materials such as the cell cortex, the spectrin cytoskeleton of red blood cells or synthetic materials such as paper sheets. In fact, much of the theoretical and simulation work on semiflexible polymer networks has been done on planar networks [3–8]; this work has shown that planar networks exhibit unique elastic properties under shear with a crossover from bending to stretching dominated elasticity, nonaffine deformation, and strain hardening. More recently, similar properties could be found in simulations of three-dimensional bulk networks, which are suitable models for bulk biopolymer gels [8–12].

Realistic 2D sheetlike materials are, however, embedded into three-dimensional space and exhibit a buckling instability with deformations normal to the initial plane resulting in wrinkling even if applied stresses are strictly in plane. All existing works on 2D semiflexible networks neglect this issue. We show that wrinkling strongly modifies the elastic properties of a 2D sheetlike material under shear in comparison to strictly planar deformations.

Wrinkling of a 2D material can occur under different loading conditions: Stretching with clamped boundaries causes tensional wrinkles along the stretching direction [13–15], and shearing gives rise to wrinkles at a 45°-angle [16, 17]. In both cases, the material is under compressive stress perpendicular to the wrinkle orientation. Here, we want to study wrinkling of 2D networks of semiflexible polymers under shear deformation in order to provide a more realistic treatment of sheet-like networks embedded into three-dimensional space, where the effects of wrinkling are of practical relevance for applications of these

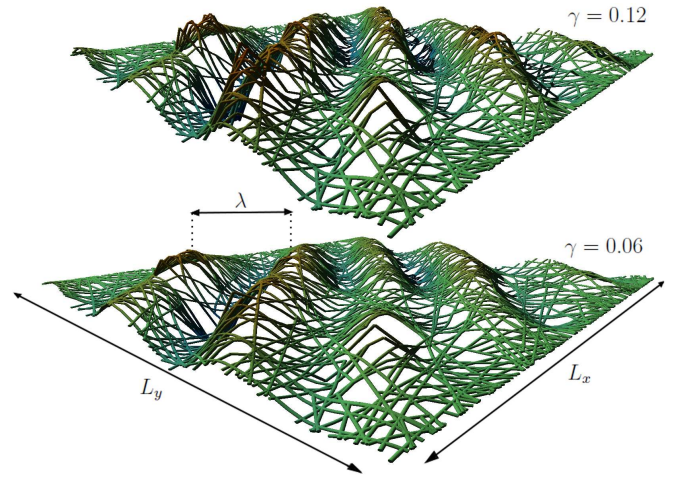


FIG. 1: Snapshots of a wrinkled random network ( $l_b/L = 2.5 \times 10^{-3}$  and  $\eta = 54$ ) at two different shear strains  $\gamma = 0.06$  and  $0.12$ . The dimensionless displacement  $z/\lambda$  in normal direction is color coded. Wrinkles form at an angle of 45° to the shearing direction; the wrinkle amplitude increases with the shear angle.

materials. We will compare regular and disordered network geometries to address the important question in the context of wrinkling theory to what extent the wrinkling instability and wrinkle properties depend on the microstructure of a material. We will compare our findings for 2D semiflexible networks to the continuum linear elasticity theory of wrinkling [16, 17].

*Model and Simulation.* Semiflexible polymer networks are generated by placing straight rods of length  $L$  into a 2D rectangular simulation cell with dimensions  $L_x \times L_y$  we use  $L_x/L = L_y/L = 1.5$  for random networks). Each rod is characterized by a stretching modulus  $\mu$  and a bending modulus  $\kappa$ . We neglect thermal fluctuations and only consider mechanical elasticity. Hence, the energy of a filament consists of a stretching energy contribution  $E^{(s)} = \int (\mu/2)[u'(s)]^2 ds$  and a bending en-

ergy contribution  $E^{(b)} = \int (\kappa/2)[\phi'(s)]^2 ds$ . Here,  $u'(s)$  is the local strain and  $\phi'(s)$  is the local curvature, both parametrized by the contour length  $s$ . The elastic moduli can be used to define the length scale  $l_b \equiv \sqrt{\kappa/\mu}$ , which can be interpreted as the “thickness” of the network as we will argue below. The number  $l_b/L$  is our dimensionless measure for the relative bending rigidity of the rods. For F-actin of length  $L = 20 \mu\text{m}$ , we typically find  $l_b/L \simeq 10^{-4}$ ; throughout the Letter, we consider comparable or higher bending rigidities  $l_b/L = 1.4 \times 10^{-4}, \dots, 2.5 \times 10^{-3}$ .

Filament intersections are identified as cross-links. During simulation, the cross-links are treated as permanent and freely rotating. Filaments exceeding the simulation cell in the  $y$  direction are fixed to the  $y$  boundaries. In the  $x$  direction, we use periodic boundary conditions. Depending on the depositing routine, two different types of 2D networks are generated: (i) The rods are either placed equidistantly at fixed orientations, resulting in a regular triangular network or (ii) added at random positions with random orientations, forming a disordered, random network. In a triangular network (i), the filaments extend through the whole simulation cell, and the lattice constant  $l_c^\Delta$  is specified to determine the total number of filaments. In a disordered network (ii), filaments are added until the network density reaches a specified value. We calculate the dimensionless network density as  $\eta = L/l_c$ . Here,  $l_c$  is the mean distance between neighboring cross-links, and  $\eta$  is equivalent to the average number of cross-links per rod. Throughout the Letter we consider densities  $\eta = 32, \dots, 54$ . For random networks, this is far above the rigidity percolation threshold, which is around  $\eta_p \simeq 6$  [18]. Based on Ref. [19], we estimate typical values for F-actin networks as  $5 \lesssim \eta \lesssim 100$ . For regular networks, we define an analogous density parameter  $\eta' = L_x/l_c^\Delta$ . In order to allow bending of the segments between cross-links, the midpoints of each segment can be displaced. With this discretization, only the first bending mode is considered, which is expected to dominate in the absence of thermal fluctuations [3].

The elastic moduli of a regular triangular network can be calculated analytically. We find a shear modulus  $G^\Delta = \sqrt{3}\mu/4l_c^\Delta$  and a Young’s modulus  $Y^\Delta = 8G^\Delta/3$  resulting in a Poisson ratio  $\nu^\Delta = 1/3$  and a bending modulus  $B^\Delta = 3G^\Delta\kappa/\mu$ . The densities of the random networks considered in this Letter are sufficiently high that the elastic moduli can be calculated by assuming affine deformations and a uniform distribution of rod orientations [3, 5]. This leads to a shear modulus  $G^r = (\pi/16)(\mu/L)(\eta + 2/\eta - 3)$  and relations for the other moduli which are identical to regular triangular networks:  $Y^r = 8G^r/3$ ,  $\nu^r = 1/3$ , and  $B^r = 3G^r\kappa/\mu$ . Using these results, we can generate regular and random networks with the same elastic moduli for comparison. Both for triangular and random networks we have  $B/3G = \kappa/\mu = l_b^2$ . In shell elasticity, the ratio  $B/3G$  is

proportional to the square of the shell thickness and in elasticity theory of thin cylindrical rods of diameter  $d$ , we have  $\kappa/\mu \sim d^2$  [20], which suggests identifying  $l_b$  with a network “thickness”.

The degrees of freedom of the simulation are the positions of cross-links and segment midpoints. Starting from an undeformed planar state, the shear deformation  $\gamma$  in the  $x$  direction is increased by small increments  $\delta\gamma$ . For each increment, we perform an affine deformation of all points, fix the  $y$  boundaries at their new positions, and find the configuration of minimal total energy using a conjugate gradient algorithm. To allow for wrinkling, we allow cross-link and midpoint positions to move in all three spatial dimensions. To avoid getting trapped in the metastable planar network configuration and enable wrinkle formation, the  $z$  coordinates (normal to the initial network plane) of cross-links and midpoints are randomly perturbed before minimization. Without this perturbation, the networks remain planar under shear, hence, they do not exhibit wrinkling. This enables us to simulate the same networks with and without wrinkling and compare their total energies  $E_{wr}$  (wrinkled) and  $E_{pl}$  (planar). Details of the simulation model are contained in the Supplemental Material [21].

*Wrinkle formation.* For shear angles  $\gamma$  exceeding a critical value  $\gamma_c$ , planar networks undergo a buckling instability, and wrinkled network configurations become energetically preferable to planar configurations. An example of a wrinkled random network is shown in Fig. 1. We find wrinkles at a  $45^\circ$  angle to the shear direction, for both triangular and random networks, i.e., independent of microstructure. For both network types, patterns with  $n$  wrinkles are well described by a displacement field  $z = A \sin(\pi y/L_y) \sin(\sqrt{2}\pi(y-x)/\lambda_n)$  normal to the  $xy$  plane with an amplitude  $A$  and wavelengths  $\lambda_n = L_x/n\sqrt{2}$ , as predicted by membrane elasticity theory [17, 21] ( $n = 3$  in Fig. 1). We focus on densities  $\eta \gtrsim 30$  because wrinkling patterns are not well defined in regions of low network density.

Continuum elasticity theory predicts a critical value  $\gamma_c \propto B/G \propto l_b^2$  for wrinkling of 2D membranes [16, 21]: Wrinkling relieves compressional stress in the direction perpendicular to the wrinkles, thus, lowering the in-plane elastic energy per area to  $e_{2D,wr} = G\gamma^2/2 - (\pi^2/2)G\gamma A^2/\lambda^2 + \mathcal{O}(A^4)$ . On the other hand, wrinkling costs an additional bending energy  $e_{B,wr} = 4\pi^4 B A^2/2[\lambda^{-4} + \lambda^{-2}L_y^{-2} + L_y^{-4}/16]$  per area. Wrinkling sets in if  $\Delta e = e_{2D,wr} + e_{B,wr} - G\gamma^2/2 < 0$  for the largest possible wavelength  $\lambda_1 = L_x/\sqrt{2}$ . This happens for

$$\gamma > \gamma_c = (4\pi^2 B/GL_y^2)[2a^2 + 1 + a^{-2}/32], \quad (1)$$

where  $a \equiv L_y/L_x$  is the aspect ratio. This energy argument also predicts a supercritical pitchfork bifurcation with  $A^2 \propto \gamma - \gamma_c$  at the onset of wrinkling, which we use to obtain  $\gamma_c$  in simulations by extrapolating  $A^2$  to zero as a function of shear angle.

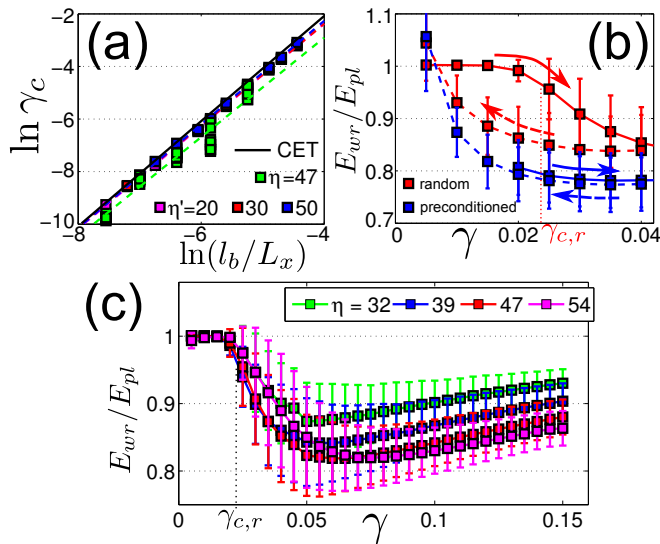


FIG. 2: (a) Critical shear angle  $\gamma_c$  as a function of the rigidity (double logarithmic) for random (densities  $\eta = 47$ ) and regular networks ( $\eta' = 20, 30, 50$ ) in comparison with linear continuum elasticity theory (CET). Lines are least square fits  $\gamma_c \propto l_b^\alpha$  (see text). (b) Total energy ratio  $E_{wr}/E_{pl}$  of wrinkled to planar networks as a function of shear angle  $\gamma$  for random networks (red) with rigidity  $l_b/L = 2.5 \times 10^{-3}$ ,  $\eta = 47$ . We find hysteresis upon reversing the deformation as indicated by the arrows. Preconditioning random networks with wrinkle patterns from regular networks results in a lower energy (blue). (c) Total energy ratio  $E_{wr}/E_{pl}$  as a function of shear angle  $\gamma$  for random networks with  $l_b/L = 2.5 \times 10^{-3}$  and  $\eta = 32, 39, 47, 54$ . Data points in (b),(c) represent averages over ten realizations, and the error bars indicate the statistical spread.

In our simulations of regular networks under shear, we confirm these results and find good agreement with (1), see Fig. 2(a). Fitting the data with a function  $\gamma_c \propto l_b^\alpha \propto (\kappa/\mu)^{\alpha/2}$  yields exponents  $\alpha = 1.93, \dots, 1.97$  depending on network density. For random networks, the situation is more complicated because we have to average over many realizations with different  $\gamma_c$ . For the average value, we find a slightly smaller exponent  $\alpha = 1.9$  for  $\eta = 47$ . Consequently,  $\gamma_c$  follows a power law as a function of  $(\kappa/\mu)$  with an exponent close to 1 in semiflexible networks as predicted by continuum elasticity theory; the dependence on network density is weak. Thus, it is a generic feature of both regular and disordered 2D semiflexible polymer networks to become unstable with respect to wrinkling already at small critical shear angles. Therefore, wrinkle formation will be relevant in most applications.

The above results were obtained using perturbations  $z$  corresponding to a sinusoidal displacement field with wavelength  $\lambda_1$ . When applying random perturbations in the  $z$  direction, wrinkling sets in at larger shear angles  $\gamma_{c,r}$  in both regular and random networks. The differ-

ence can be as large as two orders of magnitude. Additionally, we observe a hysteretic behavior at the onset of wrinkling in random networks as shown in Fig. 2(b) (red trajectory) for the total energy ratio  $E_{wr}/E_{pl}$  of wrinkled and corresponding planar networks. Shearing beyond  $\gamma_{c,r}$  and then relaxing the wrinkled state to  $\gamma < \gamma_{c,r}$ , we find that wrinkles persist as we would expect since  $\gamma_c < \gamma_{c,r}$ . Repeated simulations show that the threshold  $\gamma_{c,r}$  for wrinkling decreases for increased amplitudes of the random perturbation of the unwrinkled configuration. This effect can be explained by an energy barrier which exists between two metastable minima in the energy landscape, corresponding to the unwrinkled and wrinkled states (and exists for all  $\gamma > \gamma_c$ ). This barrier is more likely to be overcome for increased noise amplitudes.

Both planar and wrinkled 2D networks avoid compressive stress by bending. In planar networks, the individual segments bend in plane on the small scale  $l_c$  between cross-links, whereas wrinkling allows bending on larger length scales as cross-links move out of plane. As a consequence, to avoid the same amount of compressive stress, less bending energy is required in wrinkled networks, which gives rise to a lower total energy  $E_{wr} < E_{pl}$ . Figure 2(c) shows that the maximum relative energy gain by wrinkling is reached for deformations just above the threshold  $\gamma_{c,r}$  and ranges from 10% to 20% in random networks (regular networks behave qualitatively similar). At higher strains, the energy gain decreases again and  $E_{wr}/E_{pl}$  approaches unity for large  $\gamma$ . This is a characteristic feature of the nonlinear elasticity of semiflexible polymer networks with strain hardening and an elasticity dominated by the stretching of fibers along the principal strain axis at a  $45^\circ$  angle for large  $\gamma$  [7]: Whether the material wrinkles or only bends in plane in the direction perpendicular to the principal strain axis has negligible effects on the elastic energy. In a material following linear continuum elasticity theory of wrinkling, we find  $E_{wr}/E_{pl} \approx (1 + \nu)/2$  for large  $\gamma$  instead [21]. Figure 2(c) also shows that the wrinkling energy gain is larger for dense networks. An energy gain of up to 20% by wrinkling shows that wrinkling will be relevant for practically all elastic properties and that constraining sheetlike materials in simulations to planar configurations will modify material properties considerably.

In random networks, wrinkles also exhibit metastability. This is investigated using “preconditioned networks”, where we transfer the configuration of a regular network with identical elastic properties to a disordered network as the initial condition for further energy minimization. This results in lower total energies. The preconditioned networks remain energetically favorable also at higher strains, see Fig. 2(b) (blue trajectories), indicating the existence of several local minima in the energy landscape. These correspond to different metastable configurations with slightly different wrinkle configurations. Since the

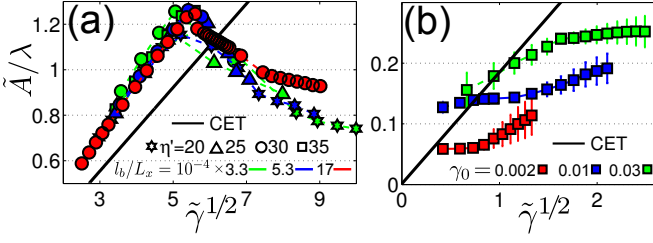


FIG. 3: Ratio of rescaled wrinkle amplitude and wavelength  $\tilde{A}/\lambda$  as a function of  $\tilde{\gamma}^{1/2}$  (a) for regular networks ( $l_b/L = 3.3, \dots, 17 \times 10^{-4}$  and  $\eta' = 20, 25, 30, 35$ ) and (b) for preconditioned random networks ( $l_b/L = 2.5 \times 10^{-3}$  and  $\eta = 39$ ). For regular networks (a), the rescaled quantities exhibit data collapse. Agreement with linear continuum elasticity theory (CET) [black line, Eq. (3)] only holds up to a maximal strain  $\tilde{\gamma}_{max}$ . For preconditioned random networks (b), rescaling does not lead to data collapse, and the amplitudes depend on the strain  $\gamma_0$  at which the networks were preconditioned.

configuration with the lowest total energy is similar in regular and disordered networks, we also conclude that the wrinkling wavelength is independent of the network microstructure.

*Wrinkle properties.* Wrinkles can be characterized by their wavelength and their amplitude. In elasticity theory of membranes, the wrinkle wavelength  $\lambda$  can be related to the applied shear. Far from the wrinkling threshold,  $\gamma \gg \gamma_c$ , the force-equilibrium in the  $z$ -direction between the outward bending forces  $\propto B\lambda\gamma^{-4}$  and the inward stretching forces  $\propto Y\gamma\lambda\gamma^{-2}$  gives [17, 21]

$$\lambda = (8\pi L_y)^{1/2} (B/Y)^{1/4} \gamma^{-1/4} = (\sqrt{72}\pi L_y l_b)^{1/2} \gamma^{-1/4} \quad (2)$$

where we used  $B/Y = 9l_b^2/8$ . With periodic boundary conditions,  $\lambda$  cannot change continuously but is restricted to discrete values  $\lambda_n = L_x/n\sqrt{2}$ . We find that regular networks follow Eq. (2) from elasticity theory within the limits of this discretization. For random networks, we find that preconditioning with the wavelength of regular networks always lowers the total energy, see Fig. 2(b). This lets us conclude that the stable wavelengths of wrinkles in random and regular networks are identical, implying validity of Eq. (2) also for random networks. Therefore, by measuring the wavelength of wrinkles, the ratio of bending to Young's/shear modulus  $B/3G = 8B/9Y = l_b^2$  or local strains  $\gamma$  can be determined via Eq. (2). This works independently of the microstructure of the network.

A second characteristic of wrinkles is their amplitude  $A$ . In continuum elasticity of membranes,  $A$  is a function of the wavelength  $\lambda$  and the applied shear strain  $\gamma$  [17, 21],

$$A = \lambda(2\pi)^{-1} \sqrt{2(1-\nu)\gamma}, \quad (3)$$

which is valid far from the wrinkling threshold. This result is obtained from linear continuum elasticity theory by assuming that wrinkling leads to a vanishing shear stress in the direction perpendicular to the wrinkles [21]. For small strains  $\gamma$ , our simulation results for wrinkled regular networks show good agreement with (3) with slightly larger amplitudes, see Fig. 3(a), which can be attributed to nonlinear effects. We find that the dependence  $A \sim \gamma^{1/2}$  only holds up to a maximum strain  $\gamma_{max}$  which depends on network density and bending stiffness, see Fig. 3(a). For  $\gamma_{max}$ , we find the empirical relation

$$\gamma_{max} \sim \xi \equiv l_b^2 l_c^{-2} \sqrt{\lambda L_y^{-1}}. \quad (4)$$

Using  $\gamma_{max} \sim \xi$  to rescale strains to  $\tilde{\gamma} = \gamma\xi^{-1}$  and amplitudes to  $\tilde{A} = A\xi^{-1/2}$ , we achieve data collapse onto a master curve with a maximum reduced amplitude at  $\sqrt{\tilde{\gamma}_{max}} \approx 5.4$ . Typical values for  $\xi$  are  $\xi = 2.9, \dots, 68 \times 10^{-5}$ . Only for values  $\tilde{\gamma} < \tilde{\gamma}_{max}$ , the wrinkle amplitude is in agreement with Eq. (3). Hence,  $\gamma_{max}$  gives an estimate for the maximum strain at which it is reasonable to treat regular networks and their wrinkles by elasticity theory. According to Eq. (2), the corresponding wavelength  $\lambda(\gamma_{max})$  only depends on  $l_c$ , which suggests that for  $\gamma > \gamma_{max}$ , the discrete network structure becomes relevant.

When comparing random networks to regular ones, we notice deviations from Eq. (3) already at smaller strains. Moreover, after being preconditioned at different strains, random networks exhibit a pronounced dependence on the initial state resulting in significantly different amplitudes as shown in Fig. 3(b). This indicates the existence of different metastable configurations differing in amplitudes despite having the same wavelength.

*Crossover from bending to stretching.* Typically, the nature of the deformation in planar random networks depends on the strain and network density. At small strains, linear elastic properties are bending dominated for small densities and become stretching dominated for higher densities [3–6]. For a fixed density, networks are bending dominated at low strains and become stretching dominated at high strains, which results in nonaffine deformations at the crossover [7]. The ratio of bending to stretching energy correlates with measures for the non-affinity of network deformation and can, thus, be used as an indicator for the transition in deformation behavior in wrinkled networks. Comparing the same networks in planar and three-dimensional simulations, we find that wrinkling causes a transition to stretching dominated behavior at much smaller strains than in planar networks. Our results suggest that the wrinkling transition inherently causes the network to become stretching dominated even if the strain is too small to cause stretching domination in a planar network. Details are included in the Supplemental Material [21].

*Conclusion.* We investigated wrinkling of two-dimensional random and triangular semiflexible polymer networks under shear. Both types of networks wrinkle already above small critical shear angles with  $\gamma_c \propto (\kappa/\mu)^{\alpha/2}$ , where  $\alpha$  ranges from 1.9 to 2.0 [see Fig. 2(a)]. Random networks exhibit hysteresis near the wrinkling threshold [see Fig. 2(b)]. The maximal energy gain upon wrinkling is up to 20%. Therefore, wrinkling is a relevant effect for all elastic properties [see Fig. 2(c)]. In random networks, we found metastable wrinkled configurations. Even though the disordered microstructure in random networks strongly affects the scaling properties of the wrinkle amplitude [see Figs. 3(a) and 3(b)], it has little effect on the wrinkle wavelength, which follows predictions from elasticity theory. Therefore, wrinkle wavelengths can represent a robust, microstructure-independent assay of shear strain or elastic properties. Wrinkling strongly affects the characteristic elastic response of 2D semiflexible polymer networks since it triggers an immediate transition to stretching dominated deformation.

*Acknowledgments.* We acknowledge financial support by the Mercator Research Center Ruhr (MERCUR).

- 
- [1] K.E. Kasza, A.C. Rowat, J. Liu, T.E. Angelini, C.P. Brangwynne, G.H. Koenderink, and D.A. Weitz, *Curr. Opin. Cell Biol.* **19**, 101 (2007).
  - [2] C. Burger, B.S. Hsiao, and B. Chu, *Annu. Rev. Mater. Res.* **36**, 333 (2006).
  - [3] D.A. Head, A.J. Levine, and F.C. MacKintosh, *Phys. Rev. Lett.* **91**, 108102 (2003).
  - [4] J. Wilhelm and E. Frey, *Phys. Rev. Lett.* **91**, 108103 (2003).
  - [5] D.A. Head, A.J. Levine, and F.C. MacKintosh, *Phys. Rev. E* **68**, 061907 (2003).
  - [6] C. Heussinger and E. Frey, *Phys. Rev. Lett.* **96**, 017802 (2006).
  - [7] P.R. Onck, T. Koeman, T. van Dillen, and E. Van der Giessen, *Phys. Rev. Lett.* **95**, 178102 (2005).
  - [8] C.P. Broedersz, X. Mao, T.C. Lubensky, and F.C. MacKintosh, *Nature Phys.* **7**, 983 (2011).
  - [9] G.A. Buxton and N. Clarke, *Phys. Rev. Lett.* **98**, 238103 (2007).
  - [10] E.M. Huisman, T. van Dillen, P.R. Onck, and E. van der Giessen, *Phys. Rev. Lett.* **99**, 208103 (2007).
  - [11] J. Blundell and E. Terentjev, *Macromolecules* **42**, 5388 (2009).
  - [12] E.M. Huisman and T.C. Lubensky, *Phys. Rev. Lett.* **106**, 088301 (2011).
  - [13] E. Cerda, K. Ravi-Chandar, L. Mahadevan, *Nature* **419**, 579 (2002).
  - [14] E. Cerda and L. Mahadevan, *Phys. Rev. Lett.* **90**, 074302 (2003).
  - [15] B. Davidovitch, R.D. Schroll, D. Vella, M. Adda-Bedia, and E. Cerda, *Proc. Natl. Acad. Sci. USA* **108**, 18227 (2011).
  - [16] S.P. Timoshenko and J.M. Gere, *Theory of Elastic Stability* (Tata McGraw-Hill Education, New Delhi, 1961).
  - [17] W. Wong and S. Pellegrino, *J. Mech. Materials Struct.* **1**, 27 (2006).
  - [18] M. Latva-Kokko and J. Timonen, *Phys. Rev. E* **64**, 066117 (2001).
  - [19] J. Liu, G.H. Koenderink, K.E. Kasza, F.C. MacKintosh, and D.A. Weitz, *Phys. Rev. Lett.* **98**, 198304 (2007).
  - [20] L. Landau and E.M. Lifshitz, *Theory of Elasticity* (Pergamon, New York, 1986).
  - [21] See Supplemental Material at <http://link.aps.org/supplemental/10.1103/PhysRevLett.112.094303> for an appendix containing a detailed description of our simulation model and summary of linear continuum elasticity theory of membrane wrinkling.